

# Anomaly in the $K_S^0 \Sigma^+$ photoproduction cross section off the proton at the $K^*$ threshold

R. Ewald<sup>a,1</sup>, A.V. Anisovich<sup>b,c</sup>, B. Bantes<sup>a</sup>, O. Bartholomy<sup>b</sup>, D. Bayadilov<sup>b,c</sup>,  
 R. Beck<sup>b</sup>, Y.A. Beloglazov<sup>c</sup>, K.-T. Brinkmann<sup>b</sup>, V. Crede<sup>b,d</sup>, H. Dutz<sup>a</sup>,  
 D. Elsner<sup>a</sup>, K. Fornet-Ponse<sup>a</sup>, F. Frommberger<sup>a</sup>, Ch. Funke<sup>b</sup>, A. B. Gridnev<sup>c</sup>,  
 E. Gutz<sup>b</sup>, W. Hillert<sup>a</sup>, J. Hannappel<sup>a</sup>, P. Hoffmeister<sup>b</sup>, I. Jaegle<sup>e</sup>, O. Jahn<sup>a</sup>,  
 T. Jude<sup>a</sup>, J. Junkersfeld<sup>b</sup>, H. Kalinowsky<sup>b</sup>, S. Kammer<sup>a,1</sup>, V. Kleber<sup>a,2</sup>, Frank  
 Klein<sup>a</sup>, Friedrich Klein<sup>a</sup>, E. Klempt<sup>b</sup>, B. Krusche<sup>e</sup>, M. Lang<sup>b</sup>, H. Löhner<sup>f</sup>,  
 I.V. Lopatin<sup>c</sup>, D. Menze<sup>a</sup>, T. Mertens<sup>e</sup>, J.G. Messchendorp<sup>f</sup>, V. Metag<sup>g</sup>,  
 M. Nanova<sup>g</sup>, V.A. Nikonov<sup>b,c</sup>, D. Novinski<sup>b,c</sup>, R. Novotny<sup>g</sup>, M. Ostrick<sup>a,3</sup>,  
 L. Pant<sup>g,4</sup>, H. van Pee<sup>b</sup>, A. Roy<sup>g,5</sup>, A.V. Sarantsev<sup>b,c</sup>, S. Schadmand<sup>g,6</sup>,  
 C. Schmidt<sup>b</sup>, H. Schmieden<sup>a,\*</sup>, B. Schoch<sup>a</sup>, S. Shende<sup>f</sup>, V. Sokhoyan<sup>b</sup>,  
 A. Süle<sup>a</sup>, V.V. Sumachev<sup>c</sup>, T. Szczepanek<sup>b</sup>, U. Thoma<sup>b</sup>, D. Trnka<sup>g</sup>,  
 R. Varma<sup>g,5</sup>, D. Walther<sup>b</sup>, Ch. Wendel<sup>b</sup>

<sup>a</sup>*Physikalisches Institut, Rheinische Friedrich-Wilhelms-Universität Bonn, Germany*

<sup>b</sup>*Helmholtz-Institut für Strahlen- u. Kernphysik, Rheinische Friedrich-Wilhelms-Universität Bonn, Germany*

<sup>c</sup>*Petersburg Nuclear Physics Institute, Gatchina, Russia*

<sup>d</sup>*Department of Physics, Florida State University, Tallahassee, USA*

<sup>e</sup>*Department of Physics and Astronomy, University of Basel, Switzerland*

<sup>f</sup>*Kernfysisch Versneller Instituut, Groningen, The Netherlands*

<sup>g</sup>*II. Physikalisches Institut, Universität Gießen, Germany*

*The CBELSA/TAPS Collaboration*

---

## Abstract

The  $\gamma + p \rightarrow K^0 + \Sigma^+$  photoproduction reaction is investigated in the energy region from threshold to  $E_\gamma = 2250$  MeV. The differential cross section exhibits increasing forward-peaking with energy, but only up to the  $K^*$  threshold. Beyond, it suddenly returns to a flat distribution with the forward cross section dropping by a factor of four. In the total cross section a pronounced structure is observed between the  $K^*\Lambda$  and  $K^*\Sigma$  thresholds. It is speculated whether this signals the turnover of the reaction mechanism from  $t$ -channel exchange below

---

\*corresponding author

*Email address:* [schmieden@physik.uni-bonn.de](mailto:schmieden@physik.uni-bonn.de) (H. Schmieden)

<sup>1</sup>now at DLR, Cologne, Germany

<sup>2</sup>now at German Research School for Simulation Sciences, Jülich, Germany

<sup>3</sup>Present address: Institut für Kernphysik, Universität Mainz, Germany

<sup>4</sup>On leave from Nucl. Phys. Division, BARC, Mumbai, India

<sup>5</sup>On leave from Department of Physics, IIT, Mumbai, India

<sup>6</sup>Present address: Institut für Kernphysik and Jülich Center for Hadron Physics, Forschungszentrum Jülich, Germany

the  $K^*$  production threshold to an  $s$ -channel mechanism associated with the formation of a dynamically generated  $K^*$ -hyperon intermediate state.

*Keywords:* meson photoproduction, strangeness, cross section, meson-baryon interaction, dynamically generated resonance

---

## 1. Introduction

The CBELSA/TAPS experiment at the Electron Stretcher Accelerator ELSA [1] of Bonn University is investigating the structure of the nucleon at low energies. The excitation spectrum provides a fingerprint of the intra-baryonic interaction dynamics in the non-perturbative regime of QCD. Lattice calculations made impressive progress over recent years and provide ab initio calculations with almost realistic quark masses of the spectrum of ground state baryon masses [2]. However, understanding excited states is still a challenge using lattice QCD, and so quark models are often used to describe the nucleon excitation spectrum. In a simple though extreme view the baryon structure is determined by a strong interaction potential which is mutually generated by the constituent quarks. While corresponding models [3, 4, 5] are successful in reproducing crucial parameters of low mass states, e.g. magnetic moments and electromagnetic couplings, important aspects of the excitation spectrum still remain dubious: (i) An essential fraction of higher mass states expected within the  $SU(6) \times O(3)$  quark models has not yet been observed. It is an open issue whether this reflects deficits of the models or of incomplete experiments. (ii) Even basic features of low-lying states are difficult to understand in genuine 3-quark models, e.g. the parity ordering of the lowest lying nucleon excitations  $N(1440)P_{11}$  (positive parity) and  $N(1535)S_{11}$  (negative parity), which naturally would be reversed in any three dimensional static potential. This is a point of controversy also in lattice QCD calculations [6, 7]. Further prominent problems are the unusually large decay into the  $\eta$  channel of the  $N(1535)S_{11}$  compared to both, the nearby angular momentum partner  $N(1520)D_{13}$  and the  $N(1650)S_{11}$  with even the same quantum numbers, or the large 115 MeV mass gap within the angular-momentum doublet  $\Lambda(1405)S_{01}$  and  $\Lambda(1520)D_{03}$ . These facts were speculated to signal other than 3-quark dynamics to affect the observed resonance structure. Associated with the spontaneous breaking of chiral symmetry, some models indeed assign an essential role for baryon dynamics to meson fields [8, 9] and meson-baryon interactions [10, 11, 12, 13, 14, 15, 16, 17, 18]. In particular in the vicinity of thresholds, the formation of (unstable) hadronic molecules in the sense of states which are dynamically generated by baryon-meson interaction is expected. They should show up, at least, as strong baryon-meson Fock components. For some low-lying states meson cloud effects seem to be indicated by meson electroproduction experiments at small momentum transfers [19], but a direct experimental observation of molecular components is still missing.

Meson photoproduction provides a sensitive tool to investigate these issues. In the experiment presented here the reaction  $\gamma p \rightarrow K^0 \Sigma^+$  was studied from

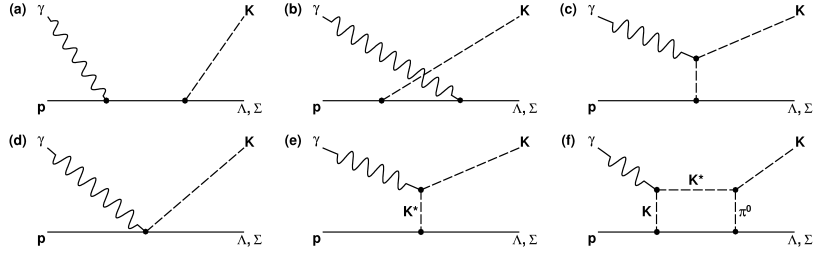


Figure 1: Diagrams contributing to charged and uncharged kaon photoproduction. The Born diagrams are shown in (a) - (d). Non-strange resonances may contribute as intermediate states in the  $s$ -channel (a) and  $u$ -channel (b). The  $t$ -channel meson exchange (c) and the seagull term (d) are proportional to the meson charge, hence contribute only to the charged kaon channel. Vector meson exchange (e) is allowed also for  $K^0$  photoproduction. Diagram (f) visualizes subthreshold  $K^*$  production with subsequent coupling into the kaon channel through  $\pi^0$  rescattering, as explained in the text.

threshold ( $E_\gamma = 1047.6$  MeV) to a photon energy of  $E_\gamma = 2250$  MeV, i.e. across the  $K^*$  production threshold at  $E_\gamma = 1678.2$  MeV for the  $K^{*+}\Lambda$  final state, and at  $E_\gamma = 1848.1$  MeV for  $K^{*0}\Sigma^+$ . Compared to charged  $K^+$  photoproduction, which has been extensively studied during recent years [20], the neutral  $K^0$  channel has tended to be sidelined. This appears entirely unjustified, though. To study  $s$ -channel resonance excitations (Figure 1(a)), the photoproduction of neutral kaons offers some advantages over charged ones, because the photons cannot directly couple to the (vanishing) charge of the meson. Hence, the  $t$ -channel diagram (c) in Figure 1 does not contribute to the production process. Since this may become dominant in charged kaon photoproduction, the neutral channel provides a cleaner probe for  $s$ -channel excitations. However,  $t$ -channel processes are not entirely suppressed in  $K^0$  photoproduction. The photon coupling to the  $K^0$ - $K^{0*}$  vertex remains non-zero and renders a  $t$ -channel exchange of a  $K^*$  meson possible as is visualised in Figure 1(e). This opens the opportunity to get a hand on explicit meson-baryon dynamics: Should  $K^*$ -hyperon dynamics play a significant role, then  $K^*$  production via diagrams of the type Figure 1(f) may yield  $K^0$  photoproduction markedly different above and below the  $K^{0*}$  threshold, unmasked by the strong charge-dominated  $t$ -exchange in  $K^+$  production. These considerations provided the motivation for our study of the  $\gamma p \rightarrow K^0 \Sigma^+$  photoproduction reaction presented here. Previous data of Crystal Barrel [21] and SAPHIR [22] agree rather well in general, however differences show up just in the energy region of the  $K^*$  threshold, prohibiting any clear conclusions on  $K^*$ -hyperon dynamics. The goal of the present experiment was to improve this unsatisfactory situation.

## 2. Experiment

The experiment was performed with the combined Crystal Barrel [23] and TAPS [24, 25] detector system at the tagged photon beam of ELSA using an

electron beam of  $E_0 = 3.2$  GeV. Bremsstrahlung was produced from a  $500 \mu\text{m}$  thick diamond crystal. Coherent bremsstrahlung peaks which carry linear polarisation were subsequently set at 1305, 1515 and 1814 MeV. For the present analysis the azimuthal distributions were summed over, however, such that the effective photon linear polarisation was zero. The bremsstrahlung electrons were momentum analysed in a magnetic dipole (tagging-) spectrometer. The spectrometer's electron detector covered a photon energy range of  $E_\gamma = 0.18\text{--}0.92E_0$ . 14 slightly overlapping scintillator bars provided the tagger timing, whereas the energy was determined by a 480 channel scintillating fibre detector at low photon energies (i.e. high rates), complemented by a MWPC at high energies (low rates). An energy resolution between 10 and 25 MeV was achieved, depending on the energy of the electron incident on the tagging detector. The tagging system was run at electron rates up to  $10^7$  Hz. The absolute photon flux was determined from the tagged electron spectrum in combination with a fast total absorbing  $\text{PbWO}_4$  detector to measure the energy dependent tagging efficiency.

The photon beam hit a 5.3 cm long liquid hydrogen target with  $80 \mu\text{m}$  Kapton windows. A three layer scintillating fibre detector (ISFD) [26] surrounded the target within the polar angular range from 15 to 165 degrees. It determined a point-coordinate for charged particles. Both, charged particles and photons, were detected in the Crystal Barrel detector. The 1290 CsI(Tl) crystals of 16 radiation lengths were arranged cylindrically around the target in 23 rings, covering a polar angular range of 30 – 168 degrees, and read out by photo diodes attached to a wavelength shifter. For photons an energy resolution of  $\sigma_E/E = 2.5\%/\sqrt[4]{E/\text{GeV}}$  and an angular resolution of  $\sigma_{\text{angle}} \simeq 1.1$  degree was obtained.

The 5.8 – 30 degree forward cone was covered by the TAPS detector, set up in one hexagonally shaped wall of 528  $\text{BaF}_2$  modules at a distance of 118.7 cm from the target. For photons between 45 and 790 MeV an energy resolution of  $\sigma_E/E = \left(0.59/\sqrt{E/\text{GeV}} + 1.9\right)\%$  was achieved. The position of photon incidence could be resolved within 20 mm. The TAPS detectors were individually equipped with photomultiplier readouts. Each TAPS module had a 5 mm plastic scintillator in front of it to measure the energy loss signal of charged particles. The first level trigger was derived from TAPS. For this purpose the detector was subdivided into 8 sectors of crystals, each provided with two discriminator thresholds. A TAPS-high trigger corresponds to at least one group above the high threshold, whereas TAPS-low requires at least two sectors above the low threshold. The thresholds were chosen as low as possible while keeping the overall TAPS trigger rate at a tolerable level of about 100 kHz. A cluster finder algorithm (FAst Cluster Encoder – FACE) for the Crystal Barrel provided a second level trigger. Here a minimum of either one or two clusters could be demanded. The detector system was read out upon one of the two global trigger conditions: (1) TAPS-low without FACE requirement or (2) TAPS-high along with FACE. In both cases, the coincidence with the tagging spectrometer was additionally required.

With the TAPS detector a 1-sigma width of 390 ps was achieved in the

time calibration for coincident photon hits in different detector modules and of 690 ps relative to the photon tagger. Starting with the energy loss induced by cosmics to set the individual high voltages, the energy calibration for both the Crystal Barrel and TAPS detectors was performed iteratively by an offline gain adjustment to minimise the width of the  $\pi^0$  peak in the 2-photon invariant mass distribution. In addition, every few hours the Crystal Barrel gains were monitored by means of a light-pulsar system with calibrated attenuators. The quality of the resulting calorimeter calibrations were then cross-checked through the width of the  $\eta$  peak in the 6-photon invariant mass spectrum. A 1-sigma width of 39 MeV was obtained. The energy calibration of the tagging system was performed by deflecting low intensity electron beams of known energy directly into the tagging detector plane. An absolute accuracy of better than 10 MeV was achieved.

### 3. Event selection and data analysis

The Crystal-Barrel/TAPS detector setup is optimised for multi-photon final states. Therefore, the  $K^0\Sigma^+$  reaction was studied in the neutral decay modes  $K^0 \rightarrow \pi^0\pi^0$  (B.R. 31.4%) and  $\Sigma^+ \rightarrow p\pi^0$  (B.R. 51.6%), which in total yields 6 photons along with the proton. Hence, event topologies with 7 cluster hits in the calorimeters were selected. Charged particles were recognised through their signals in the ISFD or the TAPS  $\Delta E$  plastic scintillators. Two charged particle events were discarded. For one charged particle in the final state the proton assignment was unique. 7 neutral cluster hits were also accepted. In this case, all combinatorial possibilities for the proton assignment were processed. The resulting combinatorial background was largely reduced through kinematic requirements in further analysis. Since the proton detection efficiency was limited, in particular at low proton momentum, 6 neutral cluster hits were also accepted.

The tagged photon energy range extended below the  $K^0\Sigma^+$  threshold. However, in the analysis a photon energy  $E_\gamma > 1047.5$  MeV was required to reduce random background. Furthermore, it was requested that 3 pairs of neutral (so-called  $\gamma$ ) hits can be found with invariant masses in the range of the  $\pi^0$ , namely  $110 \text{ MeV} \leq M_{\gamma\gamma} \leq 160 \text{ MeV}$ . The  $\eta p \rightarrow p6\gamma$  final state provided the most significant background. It was practically eliminated by requiring the invariant mass of the three identified  $\pi^0$ 's to *not* lie within the range  $470 \text{ MeV} \leq M_{\pi^0\pi^0} \leq 620 \text{ MeV}$ . This corresponds to a 4-sigma wide anticut around the  $\eta$  mass. Finally, neutral background events from the electron beamdump (which was located below the floor in front of the Crystal Barrel calorimeter) were rejected through their special angular topology.

Based on this preselection, the remaining events were subjected to a kinematic fit to the  $\gamma p \rightarrow p3\pi^0$  reaction. The photon energy was defined by the tagging spectrometer. Energy and angle parameters for the fit were provided by the final state photon hits. The proton candidate did not enter the fit. In contrast, its momentum vector was determined through the kinematic conditions. With the four components of the proton momentum to be determined

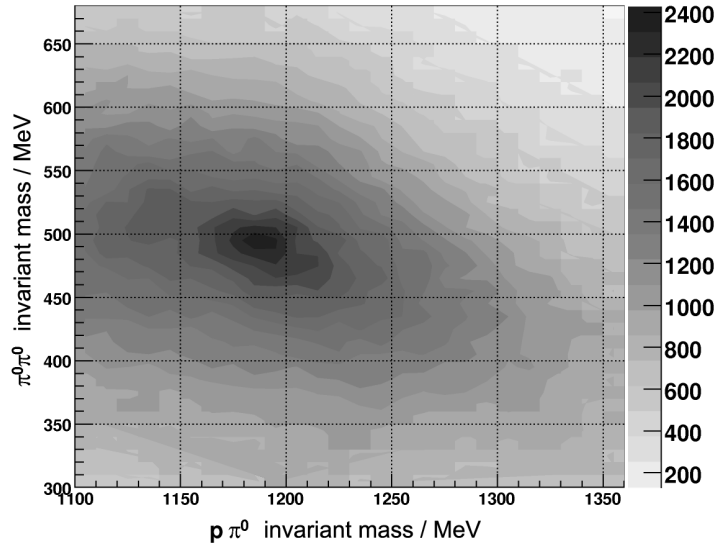


Figure 2:  $\pi^0\pi^0$  against  $p\pi^0$  invariant mass distribution after event preselection and kinematic cut, showing a concentration of events in the  $K^0\Sigma^+$  final state.

and seven conditions (overall energy-momentum and three  $\pi^0$  masses) the fit still was threefold overdetermined.  $\Sigma^+$  and  $K^0$  masses were not used as conditions of the kinematic fit. After the kinematic fit an acceptable signal to background ratio was achieved. This is demonstrated in Figure 2 where the  $2\pi^0$  invariant mass is plotted against the  $p\pi^0$  invariant mass distribution. A culmination of events is clearly visible around  $M_{\pi^0\pi^0} = 490$  and  $M_{p\pi^0} = 1190$  MeV, corresponding to the masses of  $K^0$  and  $\Sigma^+$ . As an example, Figure 3 shows the  $\pi^0\pi^0$  invariant mass distribution for the bin 1350–1450 MeV in photon energy and  $0 - 0.33$  in  $\cos\Theta_{\text{CMS}}^K$ , the kaon center-of-mass angle, after a cut on the  $\Sigma^+$  mass region in the  $p\pi^0$  mass distribution:  $1170 \text{ MeV} \leq M_{p\pi^0} \leq 1210 \text{ MeV}$ . The cut limits were obtained by minimising the related systematic error induced by background subtraction. In Monte Carlo simulations it turns out that the far dominating background is associated with uncorrelated photoproduction of three neutral pions. The simulated background distribution is shown as the hatched area in Figure 3. The spectra agree very well with the experimental distributions in all bins. The simulated yield is scaled outside the area of the  $K^0$  signal peak.

The photon energy range was divided into 12 bins of  $\pm 50$  MeV width, ranging from 1100 to 2200 MeV. Monte Carlo simulations determined the experimental acceptance individually for each of the three selected event topologies. An important benefit of the almost  $4\pi$  detection system is the practically flat acceptance. This is visualized in Figure 4.

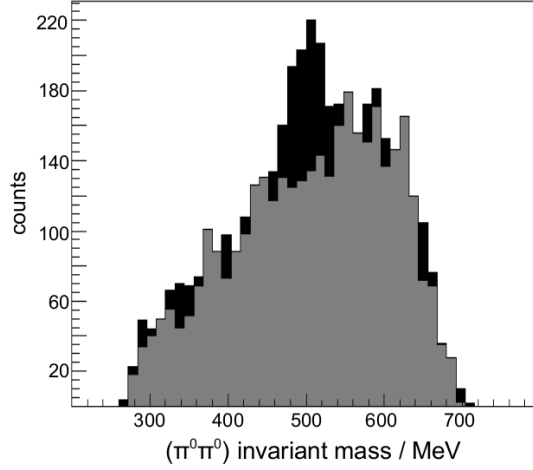


Figure 3:  $\pi^0\pi^0$  invariant mass distribution for the bin 1350 – 1450 MeV in photon energy and  $0 - 0.33$  in  $\cos\Theta_{\text{Cms}}^K$  after a cut on the  $\Sigma^+$  mass in Figure 2:  $1170 \text{ MeV} \leq M_{p\pi^0} \leq 1210 \text{ MeV}$ . The grey area represents the simulated background from uncorrelated  $3\pi^0$  photoproduction, scaled to the experimental yield outside the signal area (cf. text).

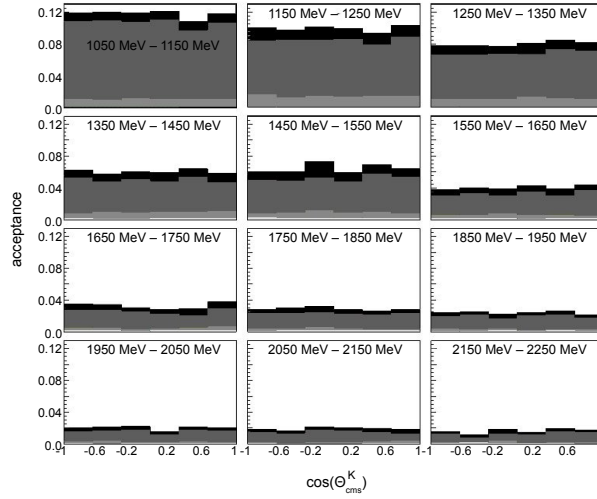


Figure 4: Simulated acceptance for the  $K^0\Sigma^+$  final state. The three event topologies are treated separately: 6 uncharged and 1 charged hits (grey), 7 uncharged hits (white), and 6 uncharged hits (light grey). The upper histogram (black) represents the total acceptance.

## 4. Results and Discussion

Based on the absolute normalisation of the photon flux provided by the tagging system, differential cross sections were determined separately for the 6 and 7 hit topologies. Both agree very well and were then combined into the full squares which are shown in Figure 5. Associated with the data points are the total statistical errors. The combined systematic error is indicated by the grey bars on the abscissa. It has contributions from the photon flux ( $\simeq 5\%$ ), the cuts applied in the analysis ( $\simeq 5 - 6\%$ ), the kinematic fit ( $\simeq 5\%$ ) and the simulated acceptance ( $\simeq 5.6\%$ ). The error of the kinematic fit is induced by a cut on the confidence level, which was required to exceed 0.1. All errors associated with cuts were estimated through the variation of the cuts over a wide range. Hence, they may be considered as upper error limits. The most probable errors would be significantly smaller. Also, the error in the photon flux affects the extracted absolute cross sections, but, within a given energy bin, it leaves the form of the angular distribution unchanged.

In comparison to our new data, Figure 5 also shows the results of previous measurements of Crystal Barrel [21] and SAPHIR [22]. While the data sets agree relatively well in general, there remain significant discrepancies in forward directions and, important for the present investigation, in the energy range of the  $K^*$  threshold ( $E_\gamma = 1750 - 1850$  MeV bin). These discrepancies could be resolved by our new data. Below the  $K^*$  threshold mostly the SAPHIR data is favored. However, at the  $K^*$  threshold and higher energies the previous Crystal Barrel data is clearly supported. The differential cross sections of a CLAS measurement presented at conferences (not shown in Figure 5) [27], which detected the charged  $K^0 \rightarrow \pi^+\pi^-$  decay, agrees well with our new data within the common detector acceptance.

As can be seen from Figure 5, directly above the  $K^0\Sigma^+$  threshold a differential cross section of  $\simeq 0.02 \mu\text{barn/sr}$  is obtained with flat angular dependence, typical for  $s$ -wave production. The cross section rises with increasing photon energy and also develops an increasing forward peaking, suggesting increasing  $t$ -channel contributions. This forward peaking is most pronounced in the  $E_\gamma = 1700 \pm 50$  MeV bin. In sharp contrast, the next energy bin exhibits an entirely flat distribution again and a drop of the cross section back to  $\simeq 0.02 \mu\text{barn/sr}$ . This is at  $E_\gamma = 1800$  MeV, i.e. right between the thresholds of  $K^*\Lambda$  and  $K^*\Sigma$  photoproduction. The differential cross section then remains almost flat and practically constant up to the highest measured energies. This suggests that in the  $K^*$  threshold region there is a sudden cross over from a  $t$ -channel mechanism back to  $s$ -channel production of  $K^0\Sigma^+$  with increasing photon energy. As is shown in Figure 6, this effect is strong enough to become clearly visible in the total cross section which, given the full  $4\pi$  acceptance, is simply obtained by integration of the differential cross sections. Due to the forward peaking of the cross section below the  $K^*$  thresholds, the effect is most pronounced in the most forward angular bin, however. Here, the cross section drops by a factor of four in the vicinity of the  $K^*$  thresholds, cf. Figure 7. It remains to be investigated whether a cusp-like structure develops, i.e. a discon-



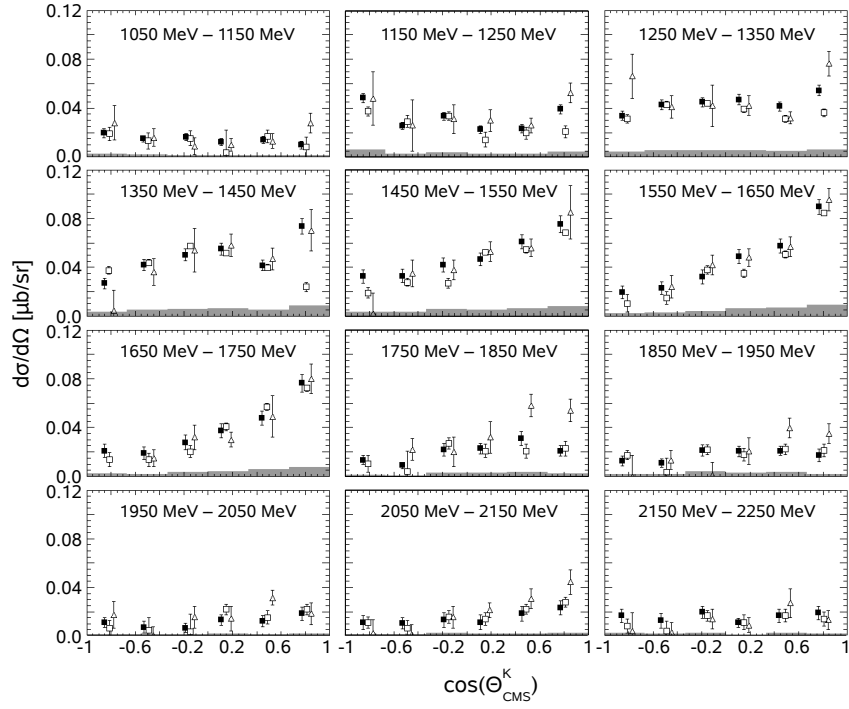


Figure 5: Measured differential cross sections for  $K^0\Sigma^+$  photoproduction as a function of the kaon center-of-mass angle in  $\pm 50$  MeV wide bins of photon energy from 1100 to 2200 MeV. The present results (full squares) are compared to previous measurements of Crystal Barrel (open squares) [21] and SAPHIR (triangles) [22]. The error bars are purely statistical. An estimate of the systematic uncertainty is given by the bars on the abscissa (cf. text).

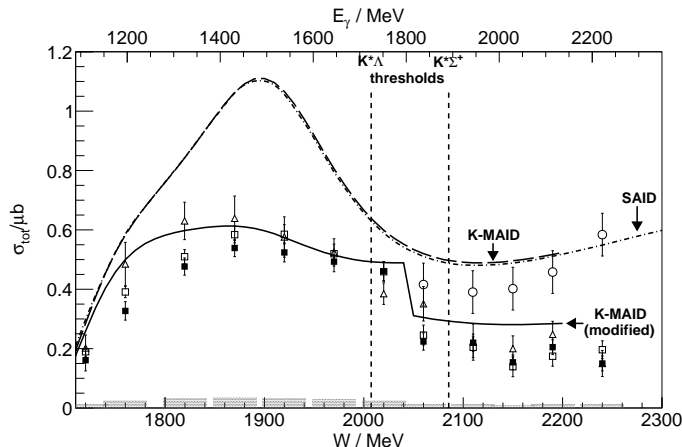


Figure 6: Total cross section for  $K^0\Sigma^+$  photoproduction as a function of the centre-of-mass energy from the present experiment (full squares) in comparison to the previous Crystal Barrel (open squares) [21] and SAPHIR (triangles) [22] data. The vertical lines indicate the  $K^*\Lambda$  and  $K^*\Sigma^+$  thresholds at  $W = 2007.4$  and  $2085.5$  MeV, respectively. The SAID parameterisation [29] is represented by the dashed-dotted curve. A K-MAID calculation with standard parameters yields the dashed curve. The full curve is obtained with the modifications described in the text. Above the  $K^*$  threshold the grey circles represent the sum of the  $K^0\Sigma^+$  cross section of the present experiment and the  $K^{0*}\Sigma^+$  cross section of the work of Nanova et al. [30]. The vertical bars on the abscissa again indicate the systematic error of the present experiment, the errors plotted with the data symbols are purely statistical.

tinuity in the slope of the cross section.

The structure seems related to a sudden change in the reaction mechanism. Below the  $K^*$  threshold, the angular distributions suggest that  $t$ -exchange according to Figure 1(e) plays a major role, which is associated with  $K^{0*}$  exchange. This hypothesis was tested with the K-MAID parameterisation [28], where it is possible to manually change the  $K^*$  exchange strength. With standard parameters both, K-MAID and SAID [29], deliver an unsatisfactory description of the data, cf. the dashed and dashed-dotted curves in Figure 6, respectively. Below the  $K^*$  threshold this can be drastically improved by adjusting the couplings of the  $S_{31}(1900)$  state to  $G_1 = 0.3$  and  $G_2 = 0.3$  [28] and reduction of the Born-couplings from 1 to 0.7. To check whether the sudden drop in the total cross section can be reproduced by changing the  $K^{0*}$  exchange, this contribution was retained below the  $K^*\Sigma^+$  threshold but manually set to zero above. As is demonstrated by the full curve in Figure 6, with these modifications K-MAID yields a significantly improved description of the cross section, including the structure at the  $K^*$  thresholds. In forward directions (cf. Figure 7) the modified K-MAID still yields unsatisfactory results at smaller energies. The drop of the cross section at the  $K^*$  thresholds is however rather well reproduced by switching off the  $K^{0*}$  exchange contribution.

In the vicinity of the threshold, a  $K^*$  would be produced almost on mass

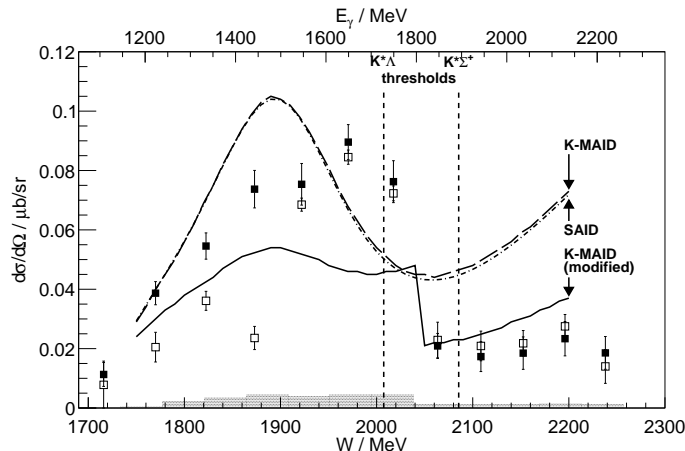


Figure 7: Cross section for  $K^0\Sigma^+$  photoproduction as a function of the centre-of-mass energy from the present (full squares) and a previous (open squares) [21] Crystal Barrel experiment in the most forward angular bin of Figure 5. Plotted errors and curves represent the same as in Figure 6, the vertical lines as well.

shell. It then strongly couples to a  $K^0$  and a pion. We speculate that, in this way, close-to-threshold  $K^*$  production feeds the  $K^0$  channel: The  $K^0$  is ejected and observed in the final state while the pion is reabsorbed by the hyperon. Such a process resembles diagram (f) of Figure 1. A vector-meson - hyperon interaction in the intermediate state is predominantly expected in a relative  $s$ -wave, which in turn would lead to the observed flat  $K^0$  angular distribution beyond the  $K^*$  thresholds.

If, above the  $K^*$  threshold, the vector meson is produced as a free particle, then diagram 1(f) no longer contributes to the  $K^0\Sigma^+$  channel. The strength, which at the dip of the cross section is vanishing from the  $K^0$  channel, is then expected to contribute to  $K^{0*}\Sigma^+$ . In order to test this idea, the measured total cross section of the reaction  $\gamma p \rightarrow K^{0*}\Sigma^+$  [30] was added to the observed  $K^0\Sigma^+$  cross section above the  $K^*$  threshold. The result is shown in Figure 6 as open circles. Using the sum of the two cross sections, a smooth transition is obtained from below to above the  $K^*$  thresholds and the dip structure vanishes. This is taken as further indication of a production mechanism as outlined above.

This discussion suggests that the situation depicted in Figure 1(f) can be seen as the coupling of the initial photon to a dynamically generated  $(K^*\Sigma)^+$  or  $(K^*\Lambda)^+$  state in the vicinity of the  $K^*$  threshold. The dip in the cross section occurs above the  $K^*\Lambda$  but *below* the  $K^*\Sigma$  threshold. This fact may indicate that indeed an intermediate state is formed with a strong  $K^*\Sigma$  component. Such states are expected in chiral unitary approaches through the interaction of the nonet of vector mesons with the octet of baryons [31]. If the vector meson and baryon couple in a relative  $s$ -wave, doublets of  $J^P = (1/2)^-$  and  $(3/2)^-$  are expected. In ref. [31] a non-strange isospin 1/2 doublet is indeed predicted at a

mass of 1972 MeV, i.e. close to the  $K^*$  threshold.

It remains to be seen whether, in a partial wave analysis (PWA), the reported structures can be reproduced by  $(1/2)^-$  and  $(3/2)^-$  partial waves. To make the PWA as unambiguous as possible, we are presently analysing polarisation observables in addition to the cross sections. In contrast to a  $t$ -channel dominated production mechanism, an  $s$ -channel intermediate state will provide a genuine spin filter. It is hence expected that, in addition to recoil polarisation and photon asymmetry, in particular the beam-target as well as the beam-recoil asymmetries will shed further light on the mechanism of  $K^0$  photoproduction in the vicinity of the observed dip structure.

The reported structure in the cross section is also close to the  $\eta'p$  threshold. In Ref. [32] a significant coupling of vectormeson-baryon to pseudoscalar-baryon channels with the same quantum numbers is expected. Consequently, one may speculate that the possible  $K^*$ -hyperon states may affect the  $\eta'p$  cross sections at threshold as well, and thus help to solve the puzzle of  $\eta'N$  interactions in both, hadronic and photoinduced reactions [32].

## 5. Summary and outlook

Using the Crystal-Barrel/TAPS detector setup at the electron accelerator facility ELSA of Bonn University, the reaction  $\gamma + p \rightarrow K^0 + \Sigma^+$  was investigated from threshold to  $E_\gamma = 2250$  MeV. We find an unexpected structure in the differential cross section between the  $K^{0*}\Lambda$  and  $K^{0*}\Sigma$  thresholds: The angular distribution exhibits a sudden transition from forward peaked to flat with increasing photon energy. In forward directions the cross section drops by a factor of four, generating a pronounced structure even in the total cross section. It is speculated that the effect may be due to close-to-threshold  $K^{0*}$  production via the formation of a  $K^*$ -hyperon quasibound state, as expected in Reference [31]. Above the  $K^*$  threshold a real  $K^*$  may be produced and the associated strength then vanishes from the  $K^0$  channel. This is supported by the total cross section of  $K^{0*}\Sigma^+$  photoproduction, which corresponds in size to the reduction of the  $K^0\Sigma^+$  cross section in the dip region.

To shed more light on the threshold structure it will be mandatory to exploit polarisation observables. In particular, the photon beam asymmetry should be sensitive to the parity character of the  $t$ -channel contributions, while recoil polarisation and beam-target asymmetry will strongly constrain the quantum numbers of an intermediate  $s$ -channel resonance. In the meanwhile polarisation observables have been measured by the collaboration and are presently under analysis. In addition, a partial wave analysis is under way where it will be interesting to see whether indications for  $(1/2)^-$  and  $(3/2)^-$  partial waves can be identified as they would be expected for a  $K^*$ - $\Lambda/\Sigma$  quasibound state.

## Acknowledgements

Helpful discussions with M. Lutz, E. Oset and A. Rusetsky are gratefully acknowledged. We thank the staff and shift-students of the ELSA accelerator

for their enthusiasm to provide an excellent beam. This work was supported by the federal state of *North-Rhine Westphalia* and the *Deutsche Forschungsgemeinschaft* within the SFB/TR-16. The Basel group acknowledges support from the *Schweizerischer Nationalfonds*,

## References

- [1] W. Hillert, Eur. Phys. J. **A 28**, s01 (2006) 139
- [2] S. Dürr et al., Science **322** (2008) 1224
- [3] A.J.G. Hey and R.L. Kelly, Phys. Report **96** (1983) 71
- [4] S. Capstick and W. Roberts, Prog. Part. Nucl. Phys. **45** (2000) 241
- [5] U. Löring, K. Kretzschmar, B.C. Metsch and H.R. Petry, Eur. Phys. J. **A 10** (2001) 309, and U. Löring, B.C. Metsch and H.R. Petry, Eur. Phys. J. **A 10** (2001) 395 and 447
- [6] N. Mathur et al., Phys. Lett **B 605** (2005) 137
- [7] Huey-Wen Lin, arXiv:1106.1608v1 [hep-lat]
- [8] L.Ya. Glozman and D.O. Riska, Physics Reports **268** (1996) 263
- [9] A. Manohar and H. Georgi, Nucl. Phys. **B 234** (1984) 189
- [10] R.H. Dalitz and J.G. McGinley, in *Low and Intermediate Energy Kaon-Nucleon Physics*, ed. by E. Ferrari and G. Violini, Reidel, Boston (1981) 381; R. H. Dalitz, T.C. Wong, and G. Rajasekaran, Phys. Rev **153** (1967) 1617
- [11] P.B. Siegel, and W. Weise, Phys. Rev **C38** (1988) 2221
- [12] N. Kaiser, T. Waas, and W. Weise, Nucl. Phys., **A 612** (1997) 297
- [13] T. Inoue, E. Oset and M. J. Vicente Vacas, Phys. Rev. C **65** (2002) 035204
- [14] T. Hyodo, S. I. Nam, D. Jido, A. Hosaka, Phys. Rev. **C68** (2003) 018201
- [15] C. Garcia-Recio, M.F.M. Lutz, and J. Nieves, Phys. Lett B 582 (2004) 49
- [16] M.F.M. Lutz and E.E. Kolomeitsev, Phys. Lett. **B 585** (2004) 243
- [17] U.-G. Meißner, U. Raha and A. Rusetsky, Eur. Phys. J. **C 35** (2004) 349
- [18] B. Borasoy et al., Eur. Phys. J. **A 34** (2007) 161
- [19] I.G. Aznauryan et al., Phys. Rev. **C 80** (2009) 055203
- [20] R. Bradford et al., Phys. Rev. **C 75** (2007) 035205
- [21] R. Castelijns et al., Eur. Phys. J. **A 35** (2008) 39

- [22] R. Lawall et al., Eur. Phys. J. **A 24** (2005) 275
- [23] E. Aker et al., Nucl. Instrum. Methods **A 321** (1992) 69
- [24] R. Novotny et al., IEEE Trans. Nucl. Sci. **38** (1991) 379
- [25] A.R. Gabler et al., Nucl. Instrum. Methods **A 346** (1994) 168
- [26] G. Suft et al., Nucl. Instrum. Methods **A 538** (2005) 416
- [27] B. Carnahan, PhD thesis, Catholic University of America, Washington D.C. (2003); see also F.J. Klein in *Proceedings of the Eighth Int. Conference on Hypernuclear and Strange Particle Physics, Newport News, VA, USA*; Ed. by A. Gal and E. Hungerford, Nucl. Phys. **A 754** (2005) 321c
- [28] <http://www.kph.uni-mainz.de/MAID/> (Version 29.3.2007)
- [29] R.A. Arndt et al., <http://gwdac.phys.gwu.edu>
- [30] M. Nanova et al. (Crystal-Barrel/TAPS Collab.), Eur. Phys. J. **A35** (2008) 333
- [31] E. Oset and A. Ramos, Eur. Phys. J. **A44** (2010) 445
- [32] E. Oset and A. Ramos, Phys. Lett. **B 704** (2011) 334